RevMexAA (Serie de Conferencias), **19**, 44–51 (2003)

DEVELOPMENT OF A GENERALIZED SCIDAR AT UNAM

D. X. Cruz,[1] S. I. González,[1] R. Avila,[2] L. J. Sánchez,[1] F. Angeles,[1] A. Iriarte,[1] L. A. Martínez,[1] S. Cuevas,[1] B. Sánchez,[1] A. Farah,[1] and M. Martínez[3]

RESUMEN

Un SCIDAR Generalizado está siendo desarrollado en la Universidad Nacional Autónoma de México, para el monitoreo de perfiles de turbulencia óptica y de velocidad del viento en sitios astronómicos. Se reportan las especificaciones, diseño y estado del proyecto. Los aspectos innovadores de este instrumento consisten principalmente en: 1) la utilización de un detector CCD de bajo ruido de lectura y alta eficiencia cuántica sin intensificador de imagen, lo cual aumenta el cociente señal a ruido y la magnitud límite de las fuentes observables con respecto a otros instrumentos tipo SCIDAR operacionales; 2) el processamiento de imágenes que se realiza en tiempo real en una computadora personal bajo el sistema operativo Linux. Paralelamente al desarrollo instrumental, un simulador numérico está siendo programado. El objetivo de dicho programa es investigar posibles efectos instrumentales. Se describe el Simulador de SCIDAR y se presentan algunos de sus resultados.

ABSTRACT

A Generalized SCIDAR is being developed at the Universidad Nacional Autónoma de México, for the monitoring of optical-turbulence profiles and wind velocity profiles at astronomical sites. We report the specifications, design and state of the project. The innovative aspects of this instrument consist mainly in: 1) the use of a low–noise and high–quantum–efficiency CCD without image intensifier, which increases the signal to noise ratio and the limiting magnitude of the observable sources compared to other operational SCIDAR instruments; 2) the image processing, which is performed in real-time on a PC under Linux operating system. Along with the instrument, a numerical simulator is being developed. The aim of this code is to investigate possible instrumental effects. The SCIDAR Simulator is described and the results obtained so far are presented.

Key Words: **ATMOSPHERIC EFFECTS — INSTRUMENTATION: HIGH ANGULAR RESOLUTION — METHODS: NUMERICAL — SITE TESTING — TECHNIQUES: HIGH ANGULAR RESOLUTION**

1. INTRODUCTION

The principal purpose of the development of a Generalized SCIDAR (GS) at the Instituto de Astronomía de la Universidad Nacional Autónoma de México is to obtain a better knowledge of atmospheric turbulence, by means of the monitoring of the optical-turbulence-strength profiles $C_{\rm N}^2(h)$ and the velocity of the optical-turbulence layers $\mathbf{v}(h)$. Of special interest is the characterization of the atmospheric turbulence at the Observatorio Astronómico Nacional at San Pedro Mártir (OAN-SPM), Mexico. Such a study provides valuable information for the development of future telescope projects.

$C_{\rm N}^2(h)$ and $\mathbf{v}(h)$ are the main physical parameters that describe the effects of atmospheric turbulence on electromagnetic waves. From these profiles, one can compute other parameters that characterize the wavefront and determine the performance of high angular resolution systems.

The turbulence and wind profiles can be measured in situ using balloon soundings. However with this technique it is not possible to follow the temporal evolution because only very few balloons can be launched per night. For the same reason one can hardly undertake a statistical study using balloon data. It is then advisable to use remote sensing techniques like SCIDAR. The SCIDAR technique allows us to obtain $C_{\rm N}^2(h)$ and $\mathbf{v}(h)$ from the statistical analysis of the scintillation pattern cast by a binary star on the pupil plane. To our knowledge, there are only three operational GS instruments, which have been developed at Nice University (France), Imperial College (UK), and the Large Binocular Telescope (USA-Italy-Germany). The Nice-University GS has been used at the OAN-SPM in 1997 and 2000, during a total of 27 nights. The results, which are presented by Avila, Vernin, & Cuevas (1998) and Avila et al. (2003), show excellent turbulence conditions at the

[1]Instituto de Astronomía, UNAM, México D.F., México.
[2]Centro de Radioastronomía y Astrofísica, UNAM, Morelia, México
[3]Facultad Ingeniería, UNAM, México D.F., México.

site, however a more complete data set is of interest to investigate, for example, seasonal trends in the turbulence profiles.

An important aspect of the development of our GS is to investigate possible instrumental effects. For this purpose the SCIDAR simulator is also being developed. This is the first publication on a simulator of a GS. The code is programmed in IDL. Presently, the physical concepts involved in the simulation of an ideal GS have been tested and the effect of the telescope aberrations has been investigated (González 2002). In the future we will incorporate telescope vibrations, intensity fluctuations and other aspects.

In § 1.1 to 1.3 the principles of the classical and generalized SCIDAR concepts are explained. The instrumental development and the SCIDAR simulator are presented in § 2 and 3. The summary and final remarks are given in § 4.

1.1. *SCIDAR Principle*

The concept of the SCIDAR Technique was proposed by Vernin & Roddier (1973) followed by interesting developments during several years (e.g. Rocca, Roddier, & Vernin [1974]) and more recently by Fuchs, Tallon, & Vernin (1998) who settled the basis for the GS, which was developed and tested by Avila, Vernin, & Masciadri (1997) and finally exploited by Avila et al. (1998) and Klückers et al. (1998). The first monitoring of velocity profiles using a GS was published by Avila, Vernin, & Sánchez (2001).

1.2. *Classical SCIDAR Concept*

Suppose, for the sake of simplicity, a unique turbulent layer at height h. A binary star with angular separation $\boldsymbol{\rho}$ projects two scintillation patterns separated by a distance $\mathbf{d} = \boldsymbol{\rho} h$ on the pupil plane of the telescope (Fig. 1). To determine the distance $\mathbf{d}$ in order to retrieve h, we compute the average autocorrelation function of the scintillation images acquired on the pupil plane. This autocorrelation is constituted by a central maximum peak and two smaller lateral peaks localized at $\mathbf{r_1} = \boldsymbol{\rho} h$ and $\mathbf{r_2} = -\boldsymbol{\rho} h$, respectively. The expression of the autocorrelation in the realistic case of multiple layers is:

$$C^{**}\left(\mathbf{r}\right) = \int_0^\infty \mathrm{d}h\, C_\mathrm{N}^2\left(h\right)\left\{a\, C\left(\mathbf{r}, h\right) + E\right\},$$
$$E = b\left[C\left(\mathbf{r} - \boldsymbol{\rho} h, h\right) + C\left(\mathbf{r} + \boldsymbol{\rho} h, h\right)\right], \tag{1}$$

where $a = \frac{1+\alpha^2}{(1+\alpha)^2}$, $b = \frac{\alpha}{(1+\alpha)^2}$, $\alpha = 10^{-0.4\Delta m}$, and Δm is the difference of the stellar magnitudes. $C\left(\mathbf{r}, h\right)$ is the autocorrelation of single-star scintillation images which can be calculated theoretically.

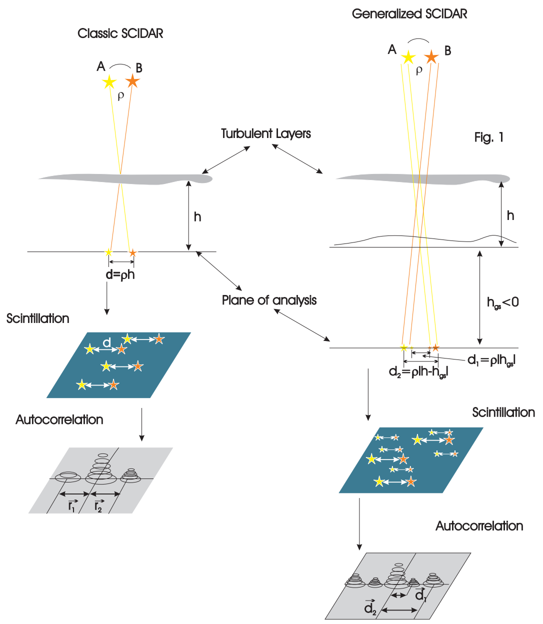

Fig. 1. Principle of Classical and Generalized SCIDAR

Notice that one of the lateral peaks is enough for retrieving $C_\mathrm{N}^2(h)$. The $C_\mathrm{N}^2(h)$ profile is retrieved from the autocorrelation using an inversion algorithm based on maximum entropy. The classical SCIDAR is insensitive to telescope aberrations and low turbulent layers. The scintillation variations produced by a layer at altitude h are proportional to $h^{5/6}$. For that reason, if images are acquired at the pupil plane, then a layer at ground level will not be detected.

1.3. *The Generalized SCIDAR concept*

In the GS, the plane of the detector is made the conjugate of a plane (analysis plane) at a distance h_gs, of the order of a few kilometers, below the telescope pupil (Fig. 1). In this case the distance relevant for scintillation produced by a turbulent layer at an altitude h is $|h - h_\mathrm{gs}|^{5/6}$, which makes the turbulence at ground level detectable. The separation of the scintillation patterns projected on the analysis plane by a double star is $|h - h_\mathrm{gs}|\, \boldsymbol{\rho}$, which is also the separation of the lateral peaks in the autocorrelation. The expression of the autocorrelation becomes in this case:

$$C_\mathrm{gs}^{**}\left(\mathbf{r}\right) = \int_0^\infty \mathrm{d}h\, C_\mathrm{N}^2\left(h\right)\left\{A + b\left[B + D\right]\right\}$$

$$A = a\, C\left(\mathbf{r}, |h - h_\mathrm{gs}|\right)$$
$$B = C\left(\mathbf{r} - \boldsymbol{\rho}\, |h - h_\mathrm{gs}|\,, |h - h_\mathrm{gs}|\right) \tag{2}$$
$$D = C\left(\mathbf{r} + \boldsymbol{\rho}\, |h - h_\mathrm{gs}|\,, |h - h_\mathrm{gs}|\right)$$

The image processing is identical to that applied

San Pedro Mártir: Astronomical Site Evaluation (México, D. F. and Ensenada, B. C., México, April 3-4, 2003)
Editors: Irene Cruz-González, Remy Avila & Mauricio Tapia

in the Classical SCIDAR case. The inversion algorithm delivers $C_N^2\,(h + h_{gs})$, from which the actual profile is deduced.

1.4. *Determination of the velocity displacement of the turbulent layers*

Imagine again a single turbulent layer at an altitude h, which is moving at a horizontal velocity $\mathbf{v}\,(h)$. Double-star scintillation-images are taken every Δt time, in the GS configuration. The speckle patterns move a distance equal to $\mathbf{v}\,(h)\,\Delta t$ from one image to the next. The mean cross-correlation of consecutive images will be constituted of the same triplet as explained above, but displaced a distance $\mathbf{v}\,(h)\,\Delta t$ from the correlation center (Fig. 2). As Δt is a known parameter, the layer velocity is deduced straightforwardly.

In the realistic case of multiple layers, the position of each triplet gives the velocity of the corresponding layer. Sometimes the triplets are superimposed which difficult the data reduction.

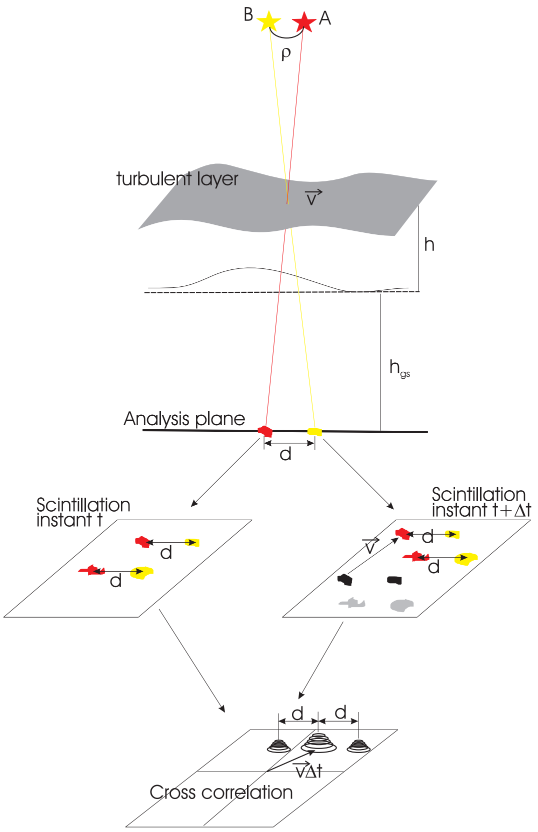

Fig. 2. Method for retrieving the velocity displacement.

2. THE GENERALIZED SCIDAR INSTRUMENT

2.1. *Generalities*

The IA-UNAM GS is based on the same concept as that of the Nice University GS (Avila et al. 1997), but uses up-to-date technology.

It consists basically of an image-acquisition system and computer processing. The principal requirements are: Short-exposure-time frames (1 ms approximately), low read-out noise, fast image transfer, near-real-time computation of the image correlations. The optics form images of a virtual plane located a few kilometers below the telescope pupil.

The images are acquired with a Marconi CCD of 80 × 80 pixels organized in 4 quadrants of 40 × 40 pixels. The quadrants are read in parallel mode. The images are digitized at 8 bits per pixel. The acquired quantity of information is equal to 6400 bytes per image organized in 32-bit words.

The *information flux* is basically the following (Fig. 3): The CCD clock signals are generated by a Texas Instrument Digital Signal Processor (TI-DSP) C31. The CCD pixel levels are pre-amplified, converted to digital signals and read by another TI-DSP C31. This procedure is performed simultaneously for the 4 quadrants of the CCD. The image is reconstructed by the TI-DSP C31 and sent to the main computer where the correlations are computed in near-real-time. The resultant correlations are sent via Ethernet to the observation computer.

The main computer is an SBC IBM PC-Compatible-Advantech equipped with an Intel Pentium !!!@800 MHz processor, 120 Mbytes of memory, Flash Disk, video card, Ethernet card and the basic ports. The whole is assembled in a panel and a Mother board with 4 ISA pipelines, in agreement with the requirements of communication, control and processing speed. A minimized version of Linux operating system is used.

The development of the system is divided in two main sections: 1) Electronics and computation; 2) mechanics and optics.

2.1.1. *Electronics and Computation*

The electronics and computation phase is constituted by the acquisition system, data transfer, data processing and user interface. The acquisition system consist of the CCD detector and data transfer. It can be subdivided in:

Pixel CCD level: Each pixel is coded in 1 byte. One pixel per quadrant is read simultaneously by the DSP. The DSP words are 32 bits long. There is a perfect match between the DSP words and the

San Pedro Mártir: Astronomical Site Evaluation (México, D. F. and Ensenada, B. C., México, April 3-4, 2003)
Editors: Irene Cruz-González, Remy Avila & Mauricio Tapia

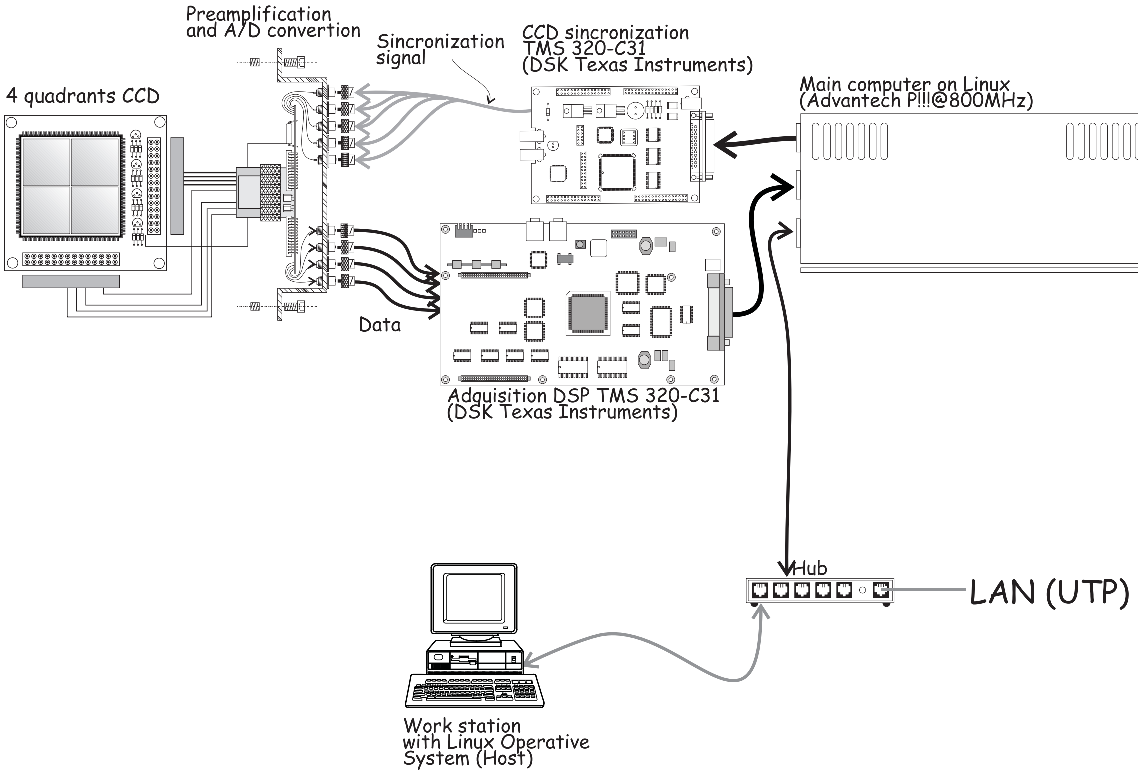

Fig. 3. Information flux diagram (See text).

4 pixels read at a time, which allow us to store the information of these 4 pixels in one DSP word.

Data processing: A certain number of consecutive images are acquired in series. The number depends on the processing speed and the available fast-access memory. As image i arrives, its Fast Fourier Transform F_i is computed. The power spectrum $\sum |F_i|^2$ and cross spectra $\sum F_i F^*_{i+1}$ and $\sum F_i F^*_{i+2}$ are then accumulated. Figure 4 shows a flow diagram of the computations.

Data transfer: Once the computation of the correlations is completed, the data is transferred and stored in the main computer.

User interface: It consists of graphical display from which the user controls the instrument parameters, its adjustment, the data acquisition and storage. The software is developed under Kylix. It is hosted on the main computer but displayed and controlled on the observer computer via an Ethernet connection.

.

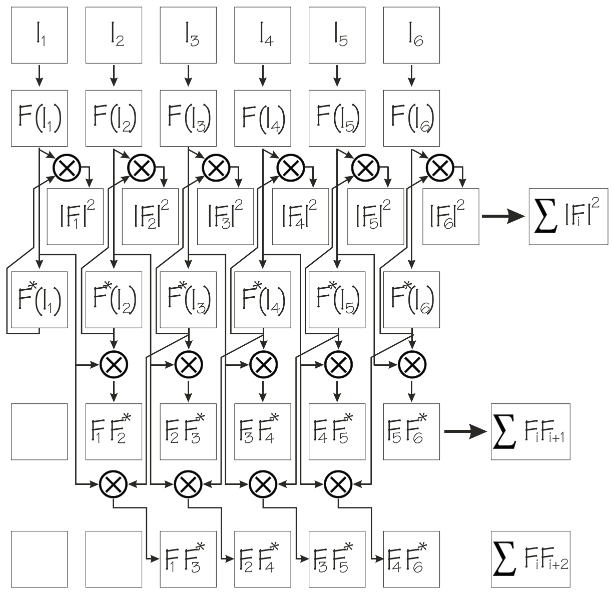

Fig. 4. Flow diagram of the data processing for the GS.

2.1.2. *Mechanics and Optics*

Mechanics: The mechanical system is shown in Figs. 5 and 6. It is constituted by: the CCD support which is mounted on a motorized sliding platform with precision positioning; a lens wheel where the different options for the collimating lens are installed; a filter wheel; an ocular for the adjustment; a support that is attached to the telescope, a cover with openings and a fan to evacuate the heat generated by the Peltier cooling system of the CCD. One

San Pedro Mártir: Astronomical Site Evaluation (México, D. F. and Ensenada, B. C., México, April 3-4, 2003)
Editors: Irene Cruz-González, Remy Avila & Mauricio Tapia

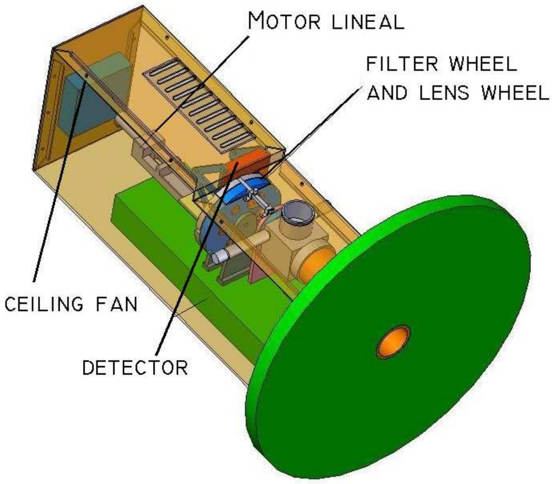

Fig. 5. Perspective view of the complete mechanical system

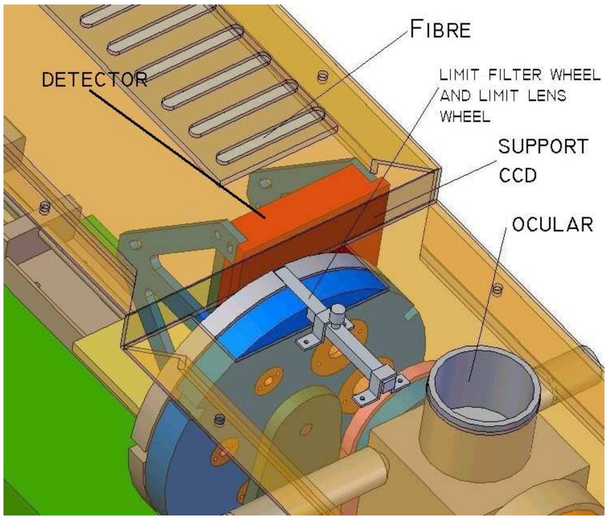

Fig. 6. Perspective view of the main functional mechanical pieces

of the constraints was that the eventual vibrations induced by the fan do not affect the observations. This requirement has been met by doing a finite element analysis of the mechanical structure.

Optics: It consists of a collimating lens (achromatic doublet), field lens, filter wheel and an ocular for adjustment. The collimating and the field lens can be changed according to the telescope and experimental setup.

2.2. *Present status*

2.2.1. *Electronics and Computation*

Detector: The detector has been tested (Fig. 7). The pre-amplification step is completed and the corresponding printed circuit is in design. The four analog/digital converters are about to be incorporated.

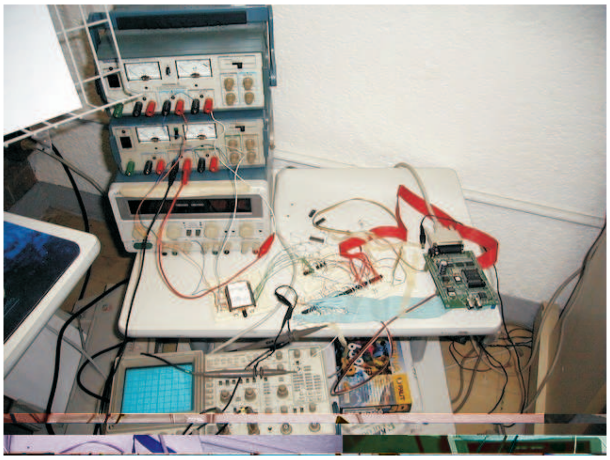

Fig. 7. *The CCD detector being tested*

Acquisition: The design and test of the acquisition board is completed (Fig. 8). The corresponding printed circuit is in the manufacture queue.

Processing software: This software is completely designed. It is in the implementation phase.

2.2.2. *Mechanics and Optics*

Mechanics: The design has been completed. The technical drawings of some pieces are ready and those of the rest are been generated to start the fabrication.

Optics: All the optical components are ready to be mounted.

3. SCIDAR SIMULATOR

The SCIDAR simulator (SS) has the ability to model the GS as well as the classical SCIDAR and some of the most important instrumental effects. It is programmed in IDL. Its code has 21 subroutines assembled in a modular form. The main program is in charge of the control of all the process and calls every subroutine.

The SS processes hundreds or thousands of amplitude and phase screens, generated by an atmospheric turbulence simulator called TurbuLenz, which was developed at the Max Planck Institut für Astronomie in Heidelberg (Germany) by Weiss et al. (2002). A large number of input images N (in the order of several hundreds or a few thousands) are necessary to reduce the numerical noise R which is proportional to $N^{-1/2}$.

3.1. *General Characteristics*

Using Turbuluenz, 1-ms-exposure-time amplitude and phase screens at the telescope-pupil level

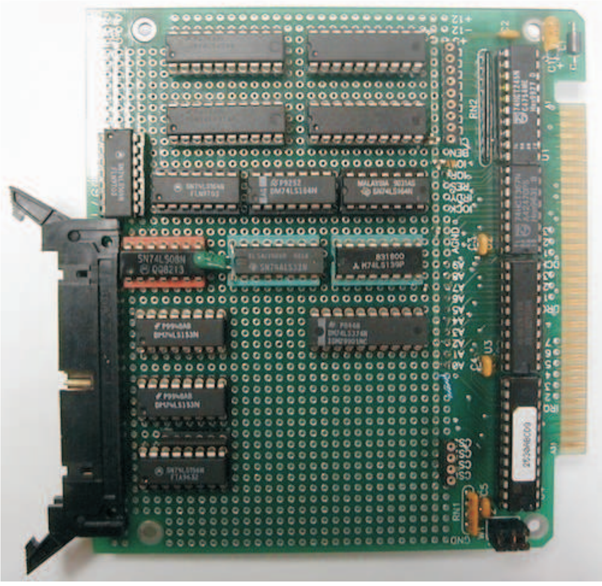

Fig. 8. *Acquisition data board tested and working, final design.*

are generated for two stars. One star is located on the optical axis and the other is displaced an angle $\boldsymbol{\rho}$. The number of turbulent layers and their characteristics (h, C_{N}^2 and $\mathbf{v}$) can be chosen at will. The screens are temporally separated by a time step of 20 ms. Many other parameters - like the pupil diameter, screen size, secondary mirror size, wave amplitude - can be modified but have been kept constant in our simulations. Each pair of phase and amplitude screens is then propagated a distance h_{gs} below the pupil using a routine based on Fresnel propagation. The resultant amplitude screens are used to calculate the mean autocorrelation and cross-correlations of the scintillation images. So far, only the effects of the telescope aberrations have been studied. The aberrations are introduced as a phase term on the pupil plane. The details of the complete procedure are explained below.

3.2. *Theoretical basis*

3.2.1. *Scintillation images*

The algorithm calculates the complex wave Ψ at the pupil plane for each star and for each time step from the amplitude A_0 and phase Φ_0 screens delivered by TurbuLenz:

$$\Psi(\mathbf{r}) = A_0(\mathbf{r}) \exp\left(\mathrm{i}\Phi(\mathbf{r})\right), \tag{3}$$

$$\Phi(\mathbf{r}) = \Phi_0(\mathbf{r}) + \Phi_{\mathrm{T}}(\mathbf{r}), \tag{4}$$

where $\Phi_{\mathrm{T}}(\mathbf{r})$ represents the first 15 Zernike polynomials of the optical aberrations of the telescope. The complex wave $\Psi_{\mathrm{gs}}(\mathbf{r})$ on the analysis plane (situated a distance h_{gs} below the pupil) is given by the convolution of $\Psi(\mathbf{r})$ with the Fresnel propagator:

$$\Psi_{\mathrm{gs}}(\mathbf{r}) = \Psi(\mathbf{r}) * \frac{1}{\mathrm{i}\lambda h_{\mathrm{gs}}} \exp\left(\mathrm{i}\,\pi \frac{\mathbf{r}^2}{\lambda h_{\mathrm{gs}}}\right), \tag{5}$$

where λ is the wavelength.

The overall inclination of the off-axis wavefront manifests itself as a phase term equal to:

$$\Phi_\rho(\mathbf{r}) = \frac{2\pi}{\lambda}\boldsymbol{\rho}\cdot\mathbf{r}. \tag{6}$$

As the distance r from the center increases, Φ_ρ rapidly reaches values much higher than 2π radians, which induces errors in the computation of the Fresnel propagation (Eq. 5). To avoid these errors, $\Phi_\rho(\mathbf{r})$ is subtracted to $\Phi(\mathbf{r})$ prior to the application of the Fresnel propagator. This removed overall tip-tilt is recovered on the propagated images by properly shifting the scintillation pattern corresponding to the off-axis star. The scintillation pattern of each star is obtained by computing the squared modulus of the corresponding complex wave. The simulation of a GS-image is the sum of the scintillation patterns arising from each star. The actual physical phenomenon consists of the sum of the complex waves. In reality, the light coming from both stars is incoherent, which prevents from any interference effect. However, interference effects may appear in the simulations as monochromatic light is considered. To avoid these artificial effects, we add the intensities and not the complex waves from each star.

3.2.2. *Autocorrelation*

Once the images on the analysis plane have been obtained, we calculate the mean autocorrelation as

$$A_I(\mathbf{r}) = \frac{1}{N}\mathcal{F}^{-1}\left[\sum_i^N \left|\mathcal{F}\left[I_i(\mathbf{r})\right]\right|^2\right], \tag{7}$$

Where $\mathcal{F}$ denotes the Fourier transform. The autocorrelation of the average image is calculated similarly:

$$A_{\langle I\rangle}(\mathbf{r}) = \mathcal{F}^{-1}\left[\left|\mathcal{F}\left[\frac{1}{N}\sum_i^N I_i(\mathbf{r})\right]\right|^2\right]. \tag{8}$$

Finally, the normalized autocorrelation is calculated as:

$$\Gamma_A(\mathbf{r}) = \frac{A_I(\mathbf{r}) - A_{\langle I\rangle}(\mathbf{r})}{A_{\langle I\rangle}(\mathbf{r})}. \tag{9}$$

San Pedro Mártir: Astronomical Site Evaluation (México, D. F. and Ensenada, B. C., México, April 3-4, 2003)
Editors: Irene Cruz-González, Remy Avila & Mauricio Tapia

San Pedro Mártir: Astronomical Site Evaluation (México, D. F. and Ensenada, B. C., México, April 3-4, 2003)
Editors: Irene Cruz-González, Remy Avila & Mauricio Tapia

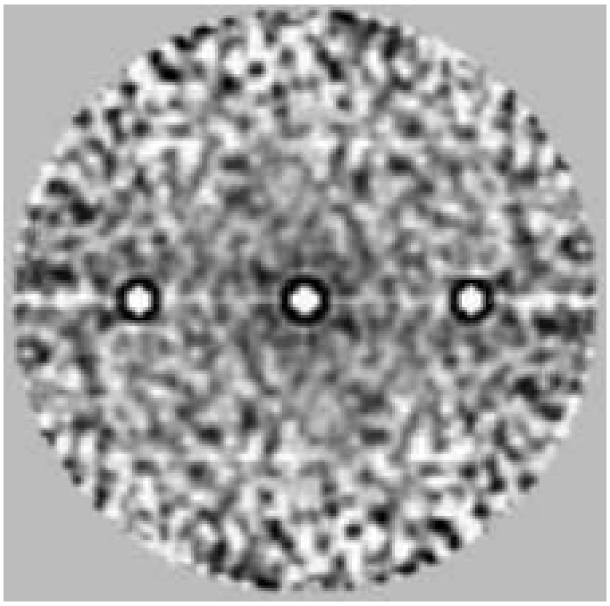

Fig. 9. Mean autocorrelation of simulated scintillation images (see text for details).

$\Gamma_A(\mathbf{r})$ is theoretically equal to $C_{\rm gs}^{**}(\mathbf{r})$, defined in Eq. 2.

An example of an autocorrelation map is shown in Fig. 9. It was obtained simulating a single turbulent layer at an altitude $h = 10$ km above the pupil. The corresponding Fried parameter (Fried 1966) is $r_0 = 15$ cm at $\lambda = 0.5$ μm. The analysis plane is located at $h_{\rm gs} = -3$ km. The pupil size is 2.1 m, and the star separation is $\rho = 10''$. The gray scale of the map is chosen such that the speckle noise is evident but the correlation peaks appear saturated. The distance between the central peak and either of the lateral peaks corresponds to $\rho(h - h_{\rm gs})$, which is the expected value. We have performed several tests on the simulated correlations. For example, we have verified that the amplitude of the correlation peaks are proportional to $(h-h_{\rm gs})^{5/6} C_{\rm N}^2(h)$ and their width are proportional to $\sqrt{\lambda(h - h_{\rm gs})}$.

3.2.3. *Cross correlations*

The mean cross correlation of images is calculated as

$$\mathcal{C}_I(\mathbf{r}) = \frac{1}{N}\mathcal{F}^{-1}\left[\sum_i^N \mathcal{F}\left[I_i(\mathbf{r})\right]\mathcal{F}\left[I_{i+s}(\mathbf{r})\right]^*\right], \quad (10)$$

where s represents the time step ($s = 1$ and $s = 2$ for time lags of 20 and 40 ms, respectively), and * represents the complex conjugate.

The normalized cross correlation is given by:

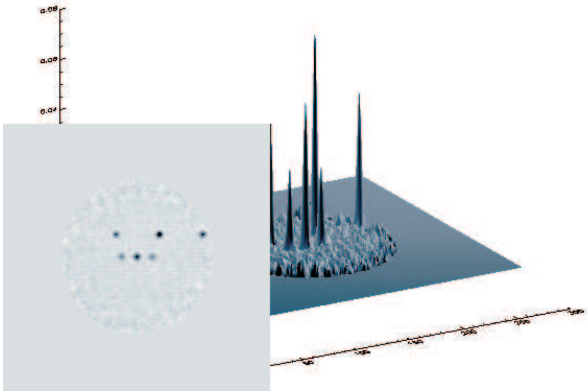

Fig. 10. Mean cross correlation of simulated scintillation images (see text for details).

$$\Gamma_{\mathcal{C}}(\mathbf{r}) = \frac{\mathcal{C}_I(\mathbf{r}) - A_{\langle I\rangle}(\mathbf{r})}{A_{\langle I\rangle}(\mathbf{r})}. \quad (11)$$

An example of a mean cross correlation map for a time lag of $\Delta t = 40$ ms is shown in Fig. 10. Two turbulent layers have been simulated with the following characteristics: $h_1 = 5$ km, $h_2 = 20$ km, $r_0 = 15$ cm for both layers, $\mathbf{v}_1 = 0$, $|\mathbf{v}_2| = 20$ m s^{-1}, $\mathbf{v}_2$ makes an angle of 45° with the horizontal axis. The altitude of the analysis plane is $h_{\rm gs} = -3$ km, the pupil size is 2.1 m, and the star separation is $\rho = 10''$. Two triplets are identified. The separation of the lateral peaks in each triplet is consistent with the corresponding layer altitude. It is also verified that the positions of the central peaks are equal to $\mathbf{v}_1\Delta t$ and $\mathbf{v}_2\Delta t$, for layers 1 and 2 respectively.

3.3. *Further developments of the SCIDAR simulator*

Instrumental effects such as telescope guidance problems and vibrations, pupil distortion, border diffraction, video noise, photon noise and dynamical aberrations can be programmed and added to the SS. Each instrumental effect will be coded as an independent module.

4. CONCLUSIONS

The GS project underway at UNAM involves instrumental development and numerical simulations.

The instrumental concept follows that of the Nice-University GS, but uses up-to-date technology as a low-noise and high-quantum-efficiency CCD, a specially designed CCD controller and real-time image processing on a PC under Linux. The UNAM GS is fully designed and is in the implementation phase. The first light is scheduled for December 2003. The instrument will be used mainly to monitor turbulence and wind profiles but can also serve as a tool for testing new techniques or perform particular experiments.

The development of the SS has been useful for testing our knowledge of the physics involved in a GS experiment. The basements of the SS have been tested and well established. The most interesting simulations are to come: the instrumental effects, which can hardly be investigated analytically.

Funding for this project has been provided by the grants J32412E from CONACyT and IN118199 from DGAPA–UNAM.

REFERENCES

Avila, R., Ibañez, F., Vernin, J., Masciadri, E., Sánchez, L. J., Azouit, M., Agabi, A., Cuevas, S., & Garfias, F. 2003, RevMexAA (SC), 19, 11

Avila, R., Vernin, J., & Masciadri, E. 1997, Appl. Opt., 36, 7898

Avila, R., Vernin, J., & Cuevas, S. 1998, PASP, 110, 1106

Avila, R., Vernin, J., & Sánchez, L. 2001, A&A, 369, 364

Fried, D. L. 1966, J. Opt. Soc. Am. A, 56, 1372

Fuchs, A., Tallon, M., Vernin, J. 1998, PASP, 110, 86

González, S. I. 2002, B. Sc. Thesis, Facultad de Ciencias, UNAM.

Klückers, V. A., Wooder, N. J., Nicholls, T. W., Adcock, M. J., Munro, I., & Dainty, J.C. 1998, A&A, 130, 41

Rocca, A., Roddier, F., Vernin, J. 1974, J. Opt. Soc. Am, 64, 1000

Vernin, J., & Roddier, F. 1973, J. Opt. Soc. Am. 63, 270

Weiss, R., et al. 2002, `http://www.mpia-hd.mpg.de/ALFA/MENU/tlz.html`

Fernando Angeles, Donají X. Cruz, Salvador Cuevas, Alejandro Farah, Sergio I. González, Arturo Iriarte, Luis Artemio Martínez, Beatriz Sánchez, Leonardo J. Sánchez: Instituto de Astronomía, Universidad Nacional Autónoma de México, Apdo. Postal 70–264, Cd. Universitaria, 04510 México D.F., México (angel,xochitl, chavoc,farah,sergio,airiarte,lamb,beatriz,leonardo@astroscu.unam.mx).

Remy Avila: Centro de Radioastronomía y Astrofísica, Universidad Nacional Autónoma de México, Apartado Postal 72–3, 58090 Morelia, Michoacán, México (r.avila@astrosmo.unam.mx).

Manuel Martínez: Facultad de Ingeniería–UNAM, Apdo. Postal 70–264, Cd. Universitaria, 04510 México D.F., México (manumarc@servidor.unam.mx).